Available online at www.sciencedirect.com
SCIENCE DIRECT
Polymer 47 (2006) 5478–5493
polymer
www.elsevier.com/locate/polymer

A low symmetry structure of isotactic poly(4-methyl-pentene-1), Form II. An illustration of the impact of chain folding on polymer crystal structure and unit-cell symmetry

J. Ruan [1], A. Thierry, B. Lotz *

Institut Charles Sadron (CNRS-ULP), 6, rue Boussingault, 67083 Strasbourg, France

Received 3 March 2005; received in revised form 20 July 2005; accepted 20 August 2005
Available online 23 May 2006

Dedicated to David Bassett on the occasion of his retirement.

Abstract

The crystal structure of the Form II modification of isotactic poly(4-methyl-pentene-1) (P4MP1) is derived by molecular mechanics modeling based on electron diffraction patterns of single crystals and on earlier X-ray powder diffraction patterns. This turns out to be a second structure derivation, since we became aware, after its completion, of the earlier work of De Rosa [De Rosa C. Macromolecules; 2003, 36, 6087] based on X-ray powder patterns and NMR data. In essential agreement with his analysis, the unit-cell is monoclinic with parameters $a=18.50$ Å, $b=10.43$ Å, $c=7.22$ Å, $\gamma=113°$. The chain has four propylene units per turn but two fold symmetry. Different structures are considered. The most straightforward ones have a space group $P2_1/a$ (c unique axis) and the cell contains two anticline enantiomorphous helices (i.e. Right up–Left down, or Right down–Left up), with possible statistical presence of up- and down-pointing helices at each helix site. However, detailed single crystal electron diffraction patterns display weak equatorial reflections that should be extinct for $P2_1/a$, indicating a lower cell symmetry. A model with $P112_1$ symmetry made of antichiral but isoclined (e.g. Right up–Left up) helices accounts better for the experimental pattern. It is suggested that this lower symmetry results from, or at least is favored by, conformational restrictions set by chain folding on the stem chirality and clinicity of helical polyolefins, as analyzed by Sadler et al. [Sadler DM, Spells SJ, Keller A, Guenet JM. Polym Commun, 25, 290, 1984] and Petraccone et al. [Petraccone V, Pirozzi B, Meille SV. Polymer, 27, 1665, 1986]: two stems linked by a fold must be either antichiral or anticline, which rules out the $P2_1/a$ symmetry. The structure taking into account the impact of folds is consistent with the single crystal habit (preferred *ac* growth planes). It corresponds to the 'chain folded lamellar' variant of the P4MP1 Form II crystal structure whereas the cells with $P2_1/a$ symmetry would be suitable models for the 'fiber' (non-folded) variant.
© 2006 Elsevier Ltd. All rights reserved.

Keywords: Crystal polymorphism; Chirality; Symmetry breaking

1. Introduction and foreword

The present paper reports the structure determination of a crystal modification of isotactic poly(4-methyl-pentene-1) (P4MP1), Form II by single crystal electron diffraction and molecular modeling that, uncharacteristically, will insist on the chronology of the process. Two features justify this approach. First, part (most?) of the structure derivation was performed while only limited (and, as it turns out, insufficient) diffraction data was available. When better data could be gathered, a more precise model could be derived, that differs by a relatively minor but important feature from the initial models. Second, after completion of the work (and when the paper was actually written!) Claudio De Rosa made us aware of his recent analysis (that had escaped our attention) of the structure of Form II based on powder diffraction patterns and NMR data [1]. Fortunately, the unit-cell and the structure are nearly identical. However, the powder X-ray diffraction pattern does not yield the additional information provided by electron diffraction, which limited De Rosa's structure analysis to the first models described in the present paper.

Since, the experimental procedures, data, determination of the cell geometry are different in the two investigations, it seems appropriate to present our work in essence as it evolved, that is, without taking into account the analysis of De Rosa.

* Corresponding author. Tel.: +33 3 88 41 40 46; fax: +33 3 88 41 40 99.
E-mail address: lotz@ics.u-strasbg.fr (B. Lotz).
[1] Present address: Institute of Materials Science and Engineering, National Sun Yat-sen University, Kaohsiung 804, Taiwan.

0032-3861/$ - see front matter © 2006 Elsevier Ltd. All rights reserved.
doi:10.1016/j.polymer.2005.08.101

Only minimal modifications have been made to our initial text, but specific sections are added in which De Rosa's results are commented. A detailed analysis of the analogies and the differences between the methods and the results will be given. It is hoped that these parallel but independent (and, in our case, belated) approaches of the same structural investigation will illustrate the diversity of methods that can be used to solve structural problems.

Isotactic poly(4-methyl-pentene-1) (P4MP1) has a crystal polymorphism that matches or even surpasses that of the better known isotactic poly(1-butene) (iPBu1). Both polyolefins can exist in three different helix conformations: 3_1, 11_3 and 4_1 for iPBu1, and 3_1, 7_2 and 4_1 for P4MP1. However, a wider range of packing schemes is observed for P4MP1.

The crystal polymorphism of P4MP1 has been established progressively (over nearly 40 years) and involves very diverse contributions. Keller et al. [2] determined the crystal structure of the stable form with 7_2 helix conformation (it was later improved by Kusanagi et al. [3]). Takayanagi et al. [4] reported on three different crystal structures with 7_2 and 4_1 helix geometries (one of which is the topic of this contribution). Charlet, Delmas and co-workers [5,6] established the existence of further crystal structures that are produced when P4MP1 is crystallized from various solvents, and using different concentrations, thermal histories, etc. De Rosa et al. established (and later refined) the crystal structure of the Form III of P4MP1 [7] using X-ray powder diffraction and selected area electron diffraction data collected by Charlet et al. [5] and Pradère et al. [8] on single crystals of this form. Rastogi et al. [9] explored the pressure–temperature phase diagram of bulk P4MP1 and confirmed the existence of a hexagonal or trigonal phase based on a 3_1 helix conformation, first proposed by Charlet and Delmas [6] and also analyzed by De Rosa [10].

Although P4MP1 has been used early on as a test material in many investigations of the structure and morphology of polyolefins crystallized both from solution [11,12] and from the bulk, some crystal modifications are not yet fully elucidated. The so-called Form II considered in the present contribution has remained very elusive for many years. In their initial reports in 1966–1967, Tagayanagi et al. [4] indicate that this form is obtained from a xylene solution quenched to room temperature (in water). They publish an X-ray powder diffraction pattern and a diffraction pattern taken from a mat of sedimented single crystals. They determine a helix conformation with four monomers per turn (which is confirmed in the present investigation) and postulate a tetragonal geometry of the unit-cell (which is not confirmed). No further progress on this crystal modification was made until the work of De Rosa mentioned earlier [1].

Our structure determination of Form II has been triggered by the availability of single crystal electron diffraction patterns that indicate a unit-cell with monoclinic geometry in chain axis projection. Combined with earlier X-ray diffraction results and information gathered on tilted single crystals, we propose a structure (derived by conformational and packing energy analysis) made of helices that have near four fold symmetry (as in Form III) but that display lower, two fold symmetry.

An interesting feature of this crystal structure of P4MP1 is the fact that the two chains in the unit-cell are not a (say) Right-handed up-pointing and a Left-handed down-pointing helix (as they would for a monoclinic $P2_1/a$ symmetry). As indicated by a number of weak equatorial reflections, the stems pack in a unit-cell with lower, $P2_1$ symmetry. It is suggested that this lower symmetry results (at least in part) from the impact of constraints set on the relative chirality and clinicity of stems linked by folds in helical polyolefins, as analyzed by Sadler et al. [13] and Petraccone et al. [14]. The crystal structure of P4MP1 Form II thus illustrates the impact of chain folding on the crystal structure symmetry, as opposed to the better documented examples of impact on unit-cell dimensions. In other words, we describe a crystal structure that may well not be a generic one, but rather is probably specific to the polymer in its chain-folded conformation.

2. Experimental procedures

The Form II of P4MP1 was obtained somewhat unintentionally when examining a thin film cast from a xylene solution and deposited on a glass slide with a doctor's blade. In our procedure, we obtained both areas with a (poorly oriented) fiber orientation of a modification with four fold helix symmetry (thus of Form III) and, embedded in a more featureless film, the crystals that yielded the *hk*0 diffraction patterns (DP) described next. In order to better characterize the morphology of the crystals that yield this DP, we attempted to reproduce the experimental conditions used by Tagayanagi et al. [4] and by Charlet and Delmas [6], but were only partially successful. Some parameters of the experimental procedure need definitely to be improved in order to better control the formation of this form. However, since we were not interested in producing whole batches of this modification, we resorted to a temperature gradient procedure. Thin films of P4MP1 were produced by depositing a few drops of a 0.15% P4MP1 solution in chlorocyclopentane between glass slide and cover slide and by letting the solvent evaporate slowly at room temperature. The film was soaked again with cyclohexane (that is most efficient to yield Form II and Form III according to Charlet and Delmas [6]), heated to 50 °C on a temperature gradient hot stage (Köfler hot stage) and the glass slide was shifted to lower temperatures where the solvent slowly evaporated and the polymer (re)crystallized. The procedure yields a significant proportion of Form III single crystals and a smaller proportion of the Form II single crystals of interest.

We could not obtain clearly recognizable fiber patterns of this form, or more exactly, we obtained mainly Form III fiber patterns. To determine the *c*-axis parameter of Form II, we relied therefore, on the published powder patterns, and on the pattern taken from a mat of sedimented single crystals published by Tagayanaki et al [4]. Some information was obtained from *hkl* reflections recorded on single crystals mounted on a rotation-tilt stage (up to $\pm 60°$).

Observations were made with a Philips CM12 electron microscope operated at 120 kV. A low beam intensity (using the defocused diffraction mode) was used in order to expand

the lifetime of the samples. The patterns were recorded with a Megaview III digital camera from soft imaging system (SIS) and analyzed with the 'AnalySIS' package. Extensive model building and packing energy analyses were performed with the Cerius2 program of Accelrys [15]. The 'Crystal Packer' and 'Minimizer' modules were extensively used, often in combination or succession. The 'Compass' and 'Universal 1.02' force fields were mostly used in the conformational and packing analyses.

3. Experimental results and derivation of the structure(s)

Analysis of the crystal structure turns out to be a very illustrative example of the need to collect sufficient experimental data in order to get insights in the details of the macromolecular and stem organization. It is most convenient to derive the crystal structure in two steps, which actually correspond to the chronology of this structure determination. In a first step, based on only limited diffraction data (cf. later, Fig. 2(a)), we derive a crystal structure (in fact two crystal structures) that obey expected rules of crystallographic symmetry. These structures are, however, only 'first order' approximations and do not account for finer details of diffraction patterns obtained later—namely some unexpected, but highly significant reflections (cf. Fig. 2(b)). In the second step of the analysis, these extra reflections are taken into account and lead to a more realistic crystal structure that actually combines elements of the two initial models. As developed in Section 4, this final structure displays characteristic features that we interpret as indicating the impact of chain folding, i.e. of a specifically macromolecular feature, on the symmetry of the unit-cell.

3.1. Unit-cell geometry and symmetry: a 'first order' approach

The original experimental findings provided by the present investigation are reported in Figs. 1 and 2. Fig. 1 illustrates a single crystal of PM4P1 Form II. It is elongated, contrary to most or all other single crystals of P4MP1 obtained so far. The major lateral growth faces, parallel to the long axis of the crystal will be indexed as (010) (*ac* faces).

Fig. 2(a) is the *hk*0 diffraction pattern obtained at first from such a single crystal a few microns in size that co-exists in our solution-cast films with less ordered domains. Fig. 2(b) is a similar single crystal diffraction pattern obtained later from the crystals produced in our temperature gradient method. Its resolution is significantly better than that of Fig. 2(a), with diffraction spots visible up to 1.7 $Å^{-1}$. This improved pattern indicates that we are dealing with the same unit-cell geometry as in Fig. 2(a), although some additional reflections (with *h* odd, circled) tell that the unit-cell symmetry is different. They will become an essential ingredient of the later analysis.

Some twinned and/or multilayered single crystals have also been observed in our samples. An example is shown in Fig. 3(a), together with the corresponding electron diffraction pattern (Fig. 3(b)). Note that some weaker diffraction spots in this pattern are even better resolved than in Fig. 2(b).

The diffraction patterns displayed in Fig. 2(a) is highly unusual when considering that it corresponds to a crystal of

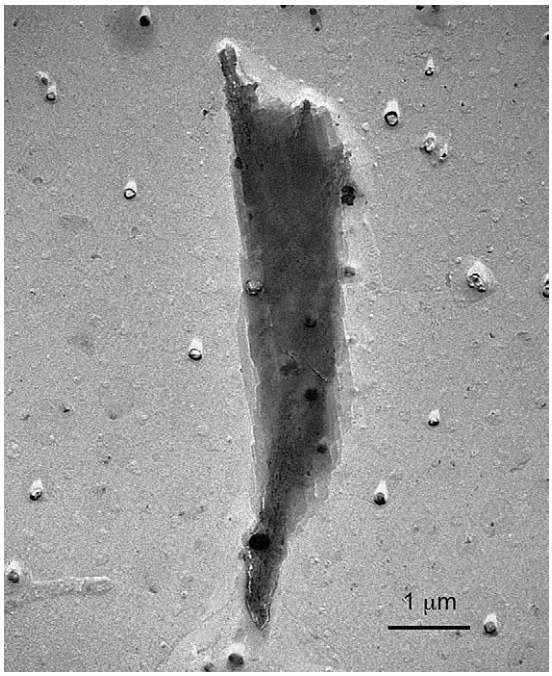

Fig. 1. A single crystal of P4MP1 Form II obtained by crystallization in thin film in the presence of cyclohexane. Electron micrograph, Pt shadowing.

P4MP1. The cell symmetry is clearly monoclinic (in chain axis projection, assuming the chain axis to be parallel to the electron beam) with (tentative) parameters $a = 9.25$ Å, $b = 10.43$ Å, $\gamma = 113°$. The spacing and relative intensities of these equatorial reflections match only one set of reflections reported for the various crystal forms of PM4P1 by Charlet and Delmas [6], namely that of Form II. The powder pattern reported by these authors (improved over that reported earlier by Takayanagi et al. [4]) is reproduced in Table 1.

The *hk*0 diffraction patterns shown in Fig. 2(a) and (b) do not provide any information on the *c*-axis parameter of the unit-cell. Fiber patterns obtained by stroking a concentrated solution in cyclohexane are of Form III. Thus far, the only available information on the *c*-axis parameter of Form II derives from a pattern taken on a mat of sedimented single crystals published by Takayanagi et al. [4]. They assign a value of 7.12 Å that indicates that the chain conformation has most likely four monomers per turn (this value was also retained by De Rosa [1]). The chain conformation thus bears strong analogies with, or at least derives from, that of Form III.

In order to evaluate by a different means this *c*-axis repeat distance, the single crystals were tilted in the electron microscope. The tilt axes were maintained parallel to the a^* and b^* axes. Since, tilt angles of 60° are accessible, it is possible to record reflections indexed as $h11$ and $1k1$. Fig. 4(a) and (b) show the diffraction patterns recorded by tilting the crystal around a^* by 35 and 60°, respectively. In Fig. 4(c) and (d), the rotation axis is b^* and tilt angles are 35 and 45°, respectively. Our results on the tilted crystals suggest a *c*-axis parameter slightly larger than that determined by Tagayanagi et al. [4]. The most decisive information stems, however, from the X-ray powder patterns reported by Charlet

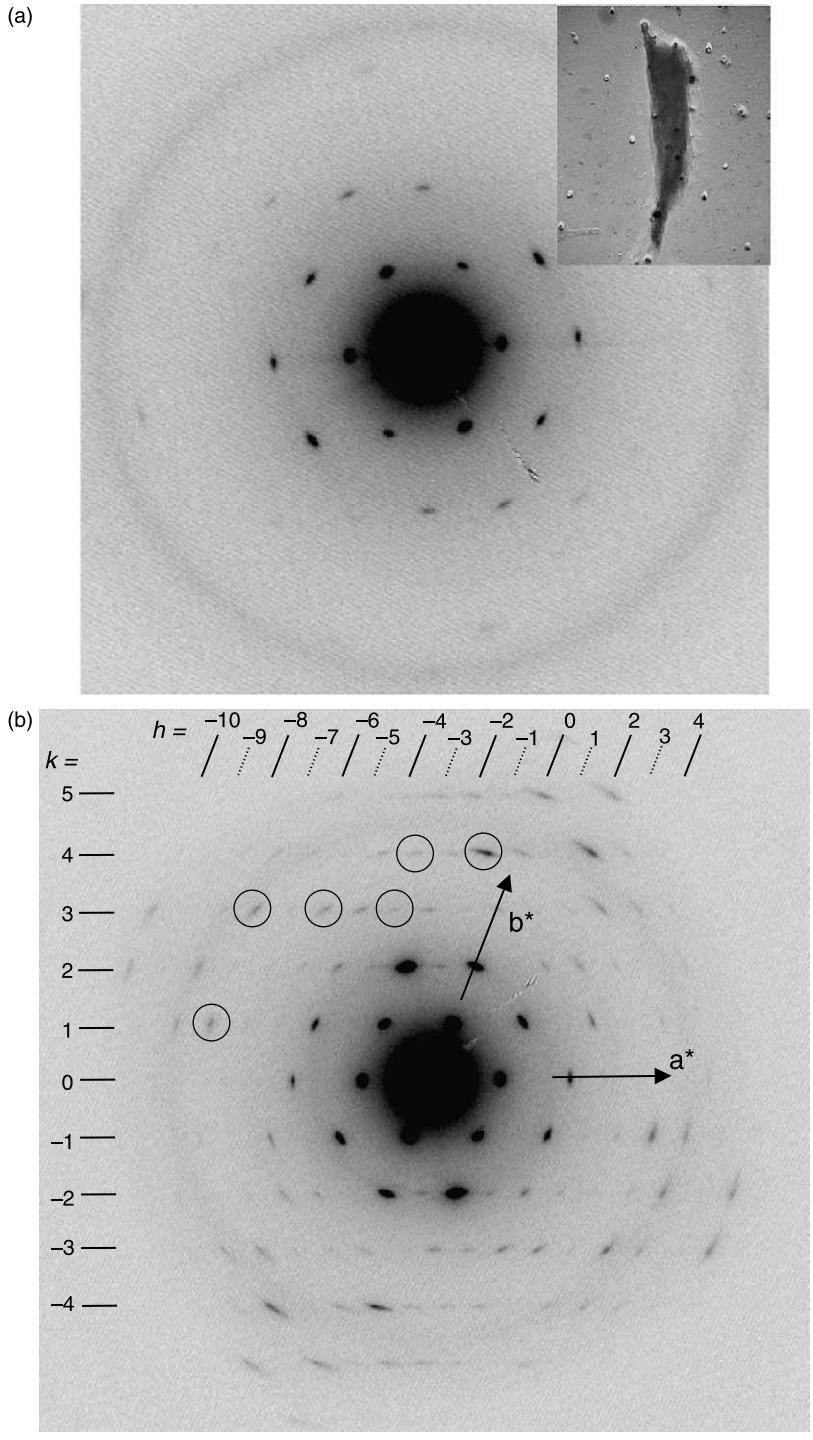

Fig. 2. (a) Electron diffraction pattern of the single crystal in Fig. 1. Inset: the crystal in proper relative orientation. (b) Improved electron diffraction pattern obtained from a larger crystal produced with the temperature gradient technique. The pattern is indexed based on the unit-cell derived in this investigation (cf. Figs. 9 and 10). Note the presence of reflections with h odd (e.g. $\bar{1}40$, $\bar{1}20$, $\bar{5}30$, $\bar{7}10$, $\bar{7}30$, etc.). These reflections impose a structure with $P112_1$ symmetry (cf. Fig. 9).

and Delmas [6], and by Takayanagi et al. [4], but only after a structural model has been derived. The three first reflections (9.50_7 Å, 8.44_3 and 6.64_4 Å, cf. Table 1) will be indexed as 010, 200 and 101, respectively. The c-axis parameter features very prominently in the computation of the latter 101 reflection, which is used therefore, to determine the most reliable value of c. For both powder patterns [4,6], the c-axis thus determined is 7.22 Å.

One further piece of information is needed in the derivation of the unit-cell dimensions. For monoclinic unit-cells, a frequent space group is number 14, $P2_1/a$ (with c as unique axis). The unit-cell has two fold screw axes and centers of symmetry, and houses two antichiral and anticline chains. Since, P4MP1 is a so-called 'chiral but racemic' polymer, it can exist as both right-handed and left-handed helices: this space group is thus a likely possibility. The c-axis projection of

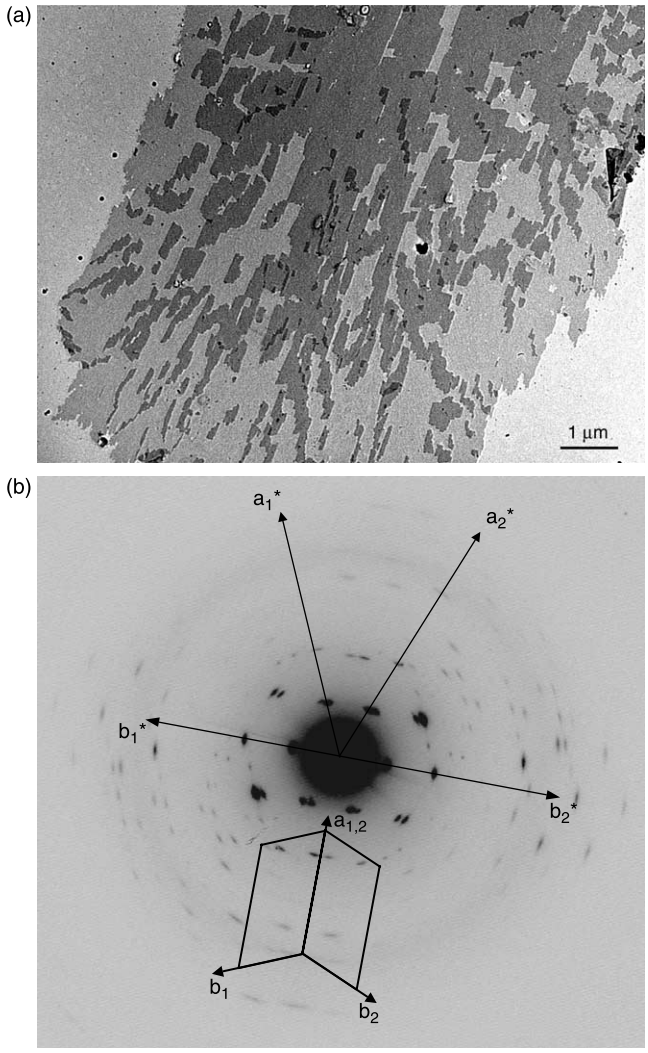

Fig. 3. Twinned and multilayered single crystal of P4MP1, Form II. (a) Bright field image (actually a defocused diffraction pattern) showing the crystal in proper relative orientation to the diffraction pattern in part (b)). (b) Electron diffraction pattern of the crystal in part (a). The unit-cells of the twinned components have been drawn on the pattern. Note that the twin plane is parallel to the *a*-axis of the unit-cell.

the two chains are, however, similar, which implies that the doubling of the unit-cell does not show up in the *hk*0 diffraction pattern, but only in the non-equatorial reflections. The diffraction patterns from tilted crystals, presented in Fig. 4, confirm that the unit-cell determined from the *hk*0 pattern shown in Fig. 2(a) should be doubled. The cell parameters are therefore: $a=18.50$ Å, $b=10.43$ Å, $c=7.22$ Å, $\alpha=\beta=90°$, $\gamma=113°$, and possible space group $P2_1/a$.

3.2. Structure derivation: 'first order' models with $P2_1/a$ symmetry

Electron diffraction on single crystals of Form II has helped establish a monoclinic unit-cell geometry. Furthermore, the *c*-axis repeat distance suggests that the chain has four monomers per turn. With these ingredients, it is possible to derive a meaningful crystal structure by relying heavily on

Table 1
X-ray powder pattern of P4MP1, Form II

Obs. d[a]	Obs.I[a]	h	k	l	d(Å)[b]	I calc. (%max)[c]
9.50_7	vs	0	1	0	9.61	52
8.44_3	s	2	0	0	8.515	100
		2	−1	0	8.14	15
6.64_4	m	1	0	1	6.65	37
5.92_6	mw	1	−1	1	5.90	45
		2	0	1	5.51	47
		2	1	0	5.41	8
5.43_6	ms	2	−1	1	5.40	94
		2	−2	0	5.125	46
5.11_1	m	1	1	1	5.11	64
4.77_7	w	0	2	0	4.80	9
4.62_4	w	4	−1	0	4.62	9
4.46_8	w	3	0	1	4.46	52
4.32_6	w	2	1	1	4.33	41
2.20_7	w					

[a] Powder pattern data (spacings, intensities) as reported by Charlet and Delmas [6].
[b] Spacings calculated for the monoclinic cell geometry determined in this work.
[c] Intensities of the most prominent reflections, calculated for the model of Fig. 9 ($P112_1$ space group). The comparison of observed and calculated *hk*0 electron diffraction intensities is displayed in Fig. 10.

conformational and packing energy analyses. This approach is fully justified since the essential characteristics of the structure are established. As illustrated indeed by Ferro et al. [16] for two polymorphs of polypivalolactone, 'computational procedures where both intra- and intermolecular actions are simultaneously taken into account within each minimization cycle… yield results in good agreement with the models directly refined by the powder X-ray profile and by electron diffraction data'. Also, we first consider structures with (ultimately incorrect) $P2_1/a$ symmetry. It was the actual structure solving chronology since, initially, we had only access to the less detailed pattern displayed in Fig. 2(a).

The backbone conformation derives from the four fold helix symmetry known from the crystal structure of the Form III, as established by De Rosa et al. [7], and our initial model borrowed indeed the conformation established in that work. A two fold symmetry is, however, more adequate, since the different inter-helix axis distances differ markedly (9.13, 10.28, and 10.75 Å along the *a* and *b* axes, and in the $(2\bar{1}0)$ plane, respectively; in the tetragonal Form III they are uniform and equal to 9.69 Å). The conformational and packing energy analyses therefore, deal mainly with the relative *c*-axis shifts of the chains, the azimuthal angle (setting angle of the chains on their axis, similar for the two chains, since in this space group they are related by a center of symmetry) and, of course, adjustments of the side- and main-chain conformations. As already indicated, this conformational and packing energy approach is first made within the confines of the $P2_1/a$ symmetry. It provides very informative insights into finer details of possible structures, but it is not the ultimate structure.

Two different structures may be considered within this simplified approach: a model with Right-up–Left-down helices and a model with Right-down–Left-up helices.

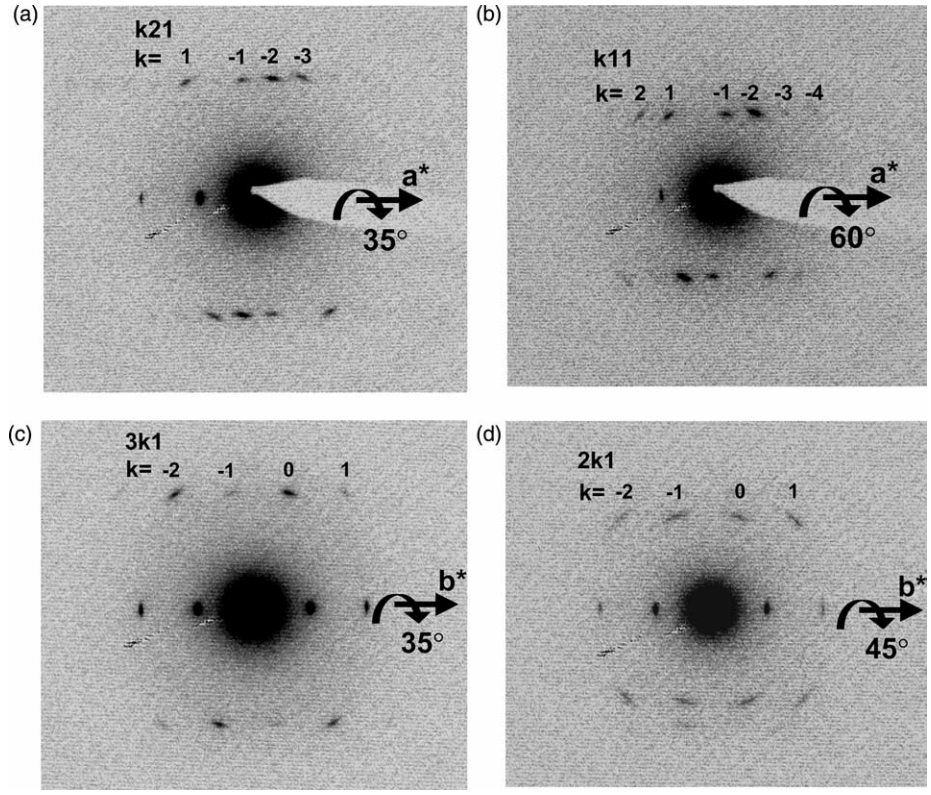

Fig. 4. Diffraction patterns obtained from tilted single crystals. The tilt axes and tilt angles are indicated, as well as the indexing of reflections. Note that rotation around the *a**-axis reveals again reflections that indicate the presence of two chains in the unit-cell.

3.2.1. Model 1 with Right-up–Left-down helices

The structure is illustrated in Fig. 5(a), as seen in *c*-axis projection. The four fold symmetry of the backbone is only slightly affected. The side-chain conformations differ to accommodate the much closer inter-chain distance in the *ac* plane but remain in the most stable conformational energy trough for P4MP1 side chains, as established by De Rosa et al. for Form III [7]. As a result, the helix symmetry is lowered to two fold. Several features of the structure are worth pointing out:

–The face-to-face packing of helices along the *a*-axis is consistent with optimized packing of enantiomorphous helices. Interdigitation of right- and left-handed paths is ensured by a *c*/2 shift of the facing side-chains. This situation is very reminiscent of the conventional packing

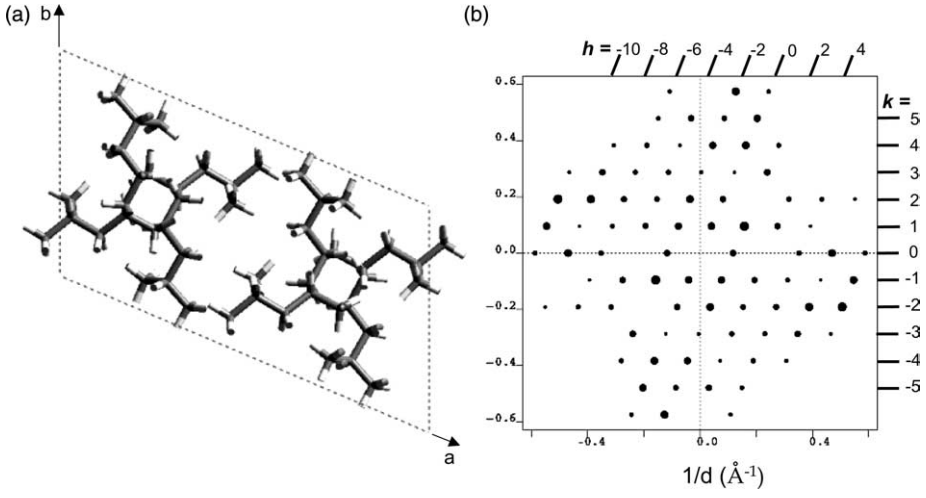

Fig. 5. Possible structures of P4MP1 with $P2_1/a$ symmetry of the unit-cell (full name: $P112_1/a$): Model 1. (a) The model with Left-down Right-up chains as seen in *c*-axis projection (Note that in this and in all subsequent models, the helix axes use the two fold screw axes of the unit-cell that are located at *b*/2 rather than 0. This option helps 'keep' the helices inside the cell). (b) Calculated electron diffraction pattern ((*hk*0) reflections). Note the absence of *hk*0 reflections with *h* odd, as expected from the cell symmetry. In all subsequent models and diffraction patterns, the cell orientation is kept constant.

Table 2

Model	Total E	van der Waals	a (Å)	b (Å)	c (Å)	γ (°)	Density
Form II $P2_1/a$ Model 1[a]	−138.5	−37.4	18.50	10.43	7.22	113	0.877
Form II $P2_1/a$ Model 2[a]	−143.4	−32.38	18.50	10.43	7.22	113	0.877
Form II $P112_1$[a]	−144.8	−33.33	18.50	10.43	7.22	113	0.877
Form III, $I4_1$[a,b]	−290.4	−78.6	19.38	19.38	6.98	90	0.853
Form III, $I4_1/a$[c]	−285.5	−67.1	19.38	19.38	6.98	90	0.853
Form II $P2_1/a$ Model 1[d]	−147.7	−38.1	17.54	10.49	6.99	113.6	0.949
Form II $P2_1/a$ Model 2[d]	−149.9	−39.89	17.46	10.81	6.79	118.0	0.959
Form II $P112_1$[d]	−149.4	−38.83	17.18	9.95	7.4	111.5	0.957
Form III, $I4_1$[b,d]	−297.2	−78.6	18.85	18.85	6.74	90	0.933
Form III, $I4_1/a$[c]	−290.9	−79.7	19.0	19.0	6.58	90	0.940

Minimizer module of Cerius 2. Bonds, angles, torsion and van der Waals terms are computed. Potentials: Compass. Energies in kcal/unit-cell.

[a] Cell parameters fixed to the experimental values determined for Forms II and III.

[b] Energies for four chains in the unit-cell (two chains for Form II).

[c] Model with anticline and antichiral chains, not retained by De Rosa et al. [7]. The azimuthal setting of the chains in the minimized structures are similar to those shown in Fig. 11(a).

[d] Variable cell parameters.

in tetragonal unit-cells of P4MP1, and most prominently its Form III (this point will be discussed later on).

–The interactions along the *b*-axis are ruled by the monoclinic cell symmetry. Helices lined up along the *b*-axis need not to be antichiral, since they are not oriented face-to-face, but rather interact through their 'corners', i.e. through one side chain only. (Fig. 5)

The exact symmetry of the cell is $P112_1/a$ (space group 14, option 4) Figs. 7(a) and 8(a). There are no short inter-atomic distances in the structure. As expected, the calculated density is rather low (0.877 g/cm^3), in line with the notoriously low crystal densities of the various forms of P4MP1. The structure corresponds to a minimum (at least local) when using the 'Minimizer' module of Cerius2 (cf. Table 2). The calculated diffraction pattern (Fig. 5(b), *hk*0 pattern) compares qualitatively well with the observed pattern, at least that shown in Fig. 2(a). It accounts in particular for the observed variation of major *h*10 reflections (strong, weak, strong, weak) or the variation of *h*00 reflections (weak 300 and 400). It is not worth pursuing, however, this comparison with experimental data, for reasons that will become clear in later sections.

3.2.2. Model 2 with Left-up–Right-down helices

A second, different model must be considered, that differs by the clinicity, i.e. by the sense (up or down) of the stems in the unit-cell. We recall that the clinicity in isotactic polyolefins is defined by the conformation rather than by the chemical structure (the latter characterizes parallel or antiparallel chains as e.g. in polypeptides or polyamide 6). In polyolefins, the side chain leaves the main chain at an angle to the helix axis, much like herringbones. The relative clinicity of two stems is defined by the relative orientation of these herringbones (cf. later, Fig. 12).

The structure of Form II just derived (Fig. 5(a)) associates a Left-down and a Right-up helix: the two helices are both enantiomorphous (antichiral) and anticline. The two helices are similar in chain axis projection. What if the clinicity of the helices were reversed, i.e. if the two helices were a Right-down and a Left-up? As shown in Fig. 6, reversing the orientation of both helices can be achieved simply by rotating the unit-cell around say its *b*-axis by 180°, that is, by looking at the unit-cell along the $-c$-axis rather than $+c$. In doing so, Left-down Right-up (Fig. 6(b)) is perceived as Left-up Right-down (Fig. 6(a)), but the structure is the same. However, the orientation of the *a*-axis has changed: the unit-cell appears, in *c*-axis projection, in twinned relationship with the initial unit-cell (Fig. 6(a) and (b)). This simple operation demonstrates that because of the low monoclinic unit-cell symmetry, the combination Left-down Right-up is not equivalent to the combination Left-up Right-down (Fig. 6(c)), when considering a unit-cell with a given *a*-axis orientation (Fig. 6(b) and (c)). This alternative model needs also be considered in the structure derivation.

We have constructed different models of the alternative unit-cell. Fig. 7 shows a model arrived at by energy minimization. The difference between the two models is best perceived by considering the location of the bond that links the side chain to the main chain, in particular near the γ monoclinic angle: anticline isochiral helices have different *c*-axis projections. The diffraction pattern of this model (Fig. 7(b)) displays (expectedly) differences in the distribution of intensities with the pattern shown in Fig. 5(b). However, and again, we compare a calculated diffraction pattern that assumes perfect $P2_1/a$ symmetry (and therefore, features no *hk*0 reflections with *h* odd) with an experimental pattern that, as seen later, corresponds to a different structure. Indeed, the actual pattern does contain *hk*0 reflections with *h* odd, which tells that the actual crystal structure differs from those considered so far.

Model II, as derived here, appears to be energetically more favorable than Model I (cf. Table 2, second line). Of course, combinations of slightly different side chain conformations, azimuthal settings of the helices, etc. are possible, and the outcome of the search depends to some extent on the vagaries of the minimization procedure. Nevertheless, the lower energy of Model II indicates that the combined chirality/clinicity Right down–Left up of the helical stems is more likely to generate the

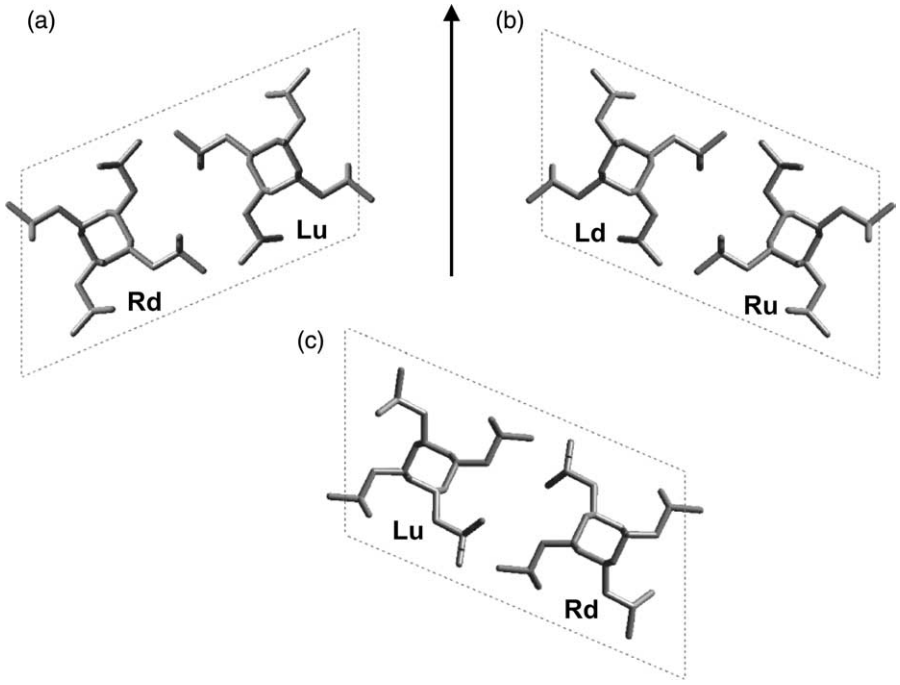

Fig. 6. The need to consider two different unit-cells with $P2_1/a$ symmetry. The model shown in Fig. 5 is represented in (b). Applying a two fold axis symmetry (indicated) to this unit-cell results in a structure (a) with Left-up Right-down helices and with different orientation of the *a*-axis (in apparent twin relationship). A different model with Left-up Right-down helices must be considered, as shown in (c). The difference between models (b) and (c) is best perceived through the side-chain oriented nearly towards the origin of the cell.

a-axis orientation of the unit-cell as shown in Figs. 5 and 7. This observation in turn suggests that a chirality/clinicity selection process of stems is likely in the development of this monoclinic structure of P4MP1. We will return to this issue when considering the final model.

3.2.3. A statistical model based on combination of unit-cells with P21/a symmetry

Before turning to this final model, we first note that the above two structures may conceivably coexist in the crystal, leading to a statistical unit-cell in which any site may be occupied by up- or- down helices, provided that they have the same chirality. Such a model, very reminiscent of the classical structure derivations of polyolefin crystal structures that assume this disorder, is represented in Fig. 8(a), together with its calculated diffraction pattern (Fig. 8(b)). Note also that the calculated pattern reproduces most of the features of the electron diffraction pattern shown in Fig. 2(a). In particular, the cell symmetry remains $P2_1/a$ and—again—all $hk0$ reflections with h odd are absent.

Summing up the features considered so far, we note that the clinicity issue, recurrent in the structure determination of

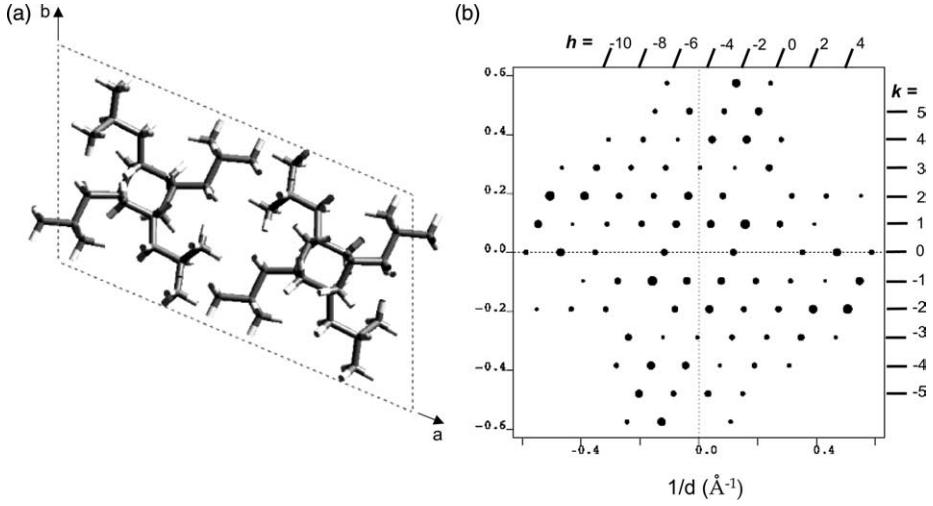

Fig. 7. Possible structures of P4MP1 with $P2_1/a$ symmetry of the unit-cell: Model 2. (a) The model, with Left-up Right-down chains. (b) Calculated electron diffraction pattern (($hk0$) reflections). Note again the absence of $hk0$ reflections with h odd.

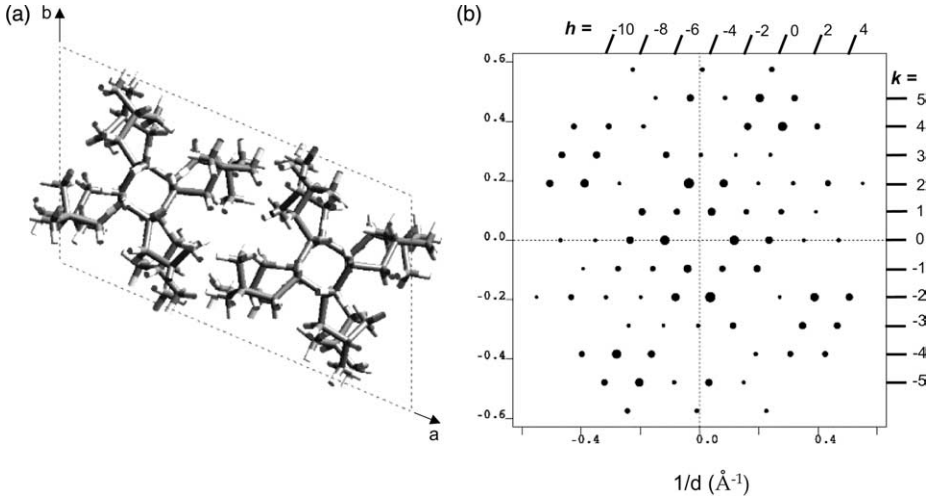

Fig. 8. Possible structures of P4MP1 with $P2_1/a$ symmetry of the unit-cell: statistical model. (a) The statistical model based combining models of Figs. 5 and 7. Each chain site is occupied by isochiral but anticline stems. (b) Corresponding calculated electron diffraction pattern ((*hk*0) reflections). In the present case, absence of *hk*0 reflections with *h* odd results from both the cell symmetry and from the fact that we are dealing with a statistical model.

polyolefins, becomes a major concern in Form II of P4MP1. As a result of the monoclinic symmetry of the unit-cell and the azimuthal setting of the helices in the cell, two different models (and their statistical combination) may be considered. Their calculated diffraction patterns differ in their details, if not in their main features, which would, in principle at least, provide a means to differentiate them in a structure derivation.

The above structure derivations yield models that satisfy most of the criteria set for acceptable crystal structures: density, absence of steric conflicts (as assessed by the low packing energies reached during the minimization process), general agreement with the experimental diffraction patterns. The stage reached so far would thus have constituted a logical outcome of the present structure derivation, had only the limited diffraction data of Fig. 2(a) been available. For many polymer crystal structures, and most prominently for unstable or metastable crystal modifications, available data are frequently limited: powder patterns only, or fiber patterns with few reflections. We recall that Cojazzi et al. [17] solved the structure of Form III of iPBu1 from a powder pattern with twelve reflections only (and thus with many overlaps), and the powder pattern of Form III of P4MP1 recorded by De Rosa et al. [7] displays only eight reflections (In both cases, however, the structure derivation led to the correct models!). It turns out, however that, for the Form II of P4MP1 considered here, the single crystal electron diffraction pattern of Fig. 2(b) tells a more complex story, as detailed next.

Before moving on, we must first stress the analogies of the structures just derived with the models proposed by De Rosa [1]. Strikingly, he was able to derive the unit-cell geometry from the powder pattern: his calculated monoclinic γ angle is 113.7° compared to 113°, measured on our *hk*0 diffraction pattern. The statistical model of Fig. 8(a) is essentially similar (except for a different choice of *a* and *b* axes) to the structure derived by De Rosa on the sole basis of the X-ray powder pattern and NMR data. However, due to the intrinsic limitations of X-ray powder diffraction on polymers, the pattern recorded by De Rosa [1] (although significantly improved over that of Charlet and Delmas [6]) does not display reflections beyond 2.7 $Å^{-1}$, i.e. just short of some critical reflections that will come into play next. Also, for large unit-cells, indexing of far out and weak reflections of the powder pattern is difficult, due to overlapping of many reflections, and the impossibility to discriminate *hk*0 from *hkl* reflections. It turns out that information provided by single crystal *hk*0 electron diffraction patterns helps refine the structural analysis performed so far.

3.3. Structure derivation: a lower symmetry model

The above crystal structures are only simplified versions of the actual structure. As already indicated, the crystal structures with $P2_1/a$ symmetry include two enantiomorphous and anticline helices. However, since the two helices have identical

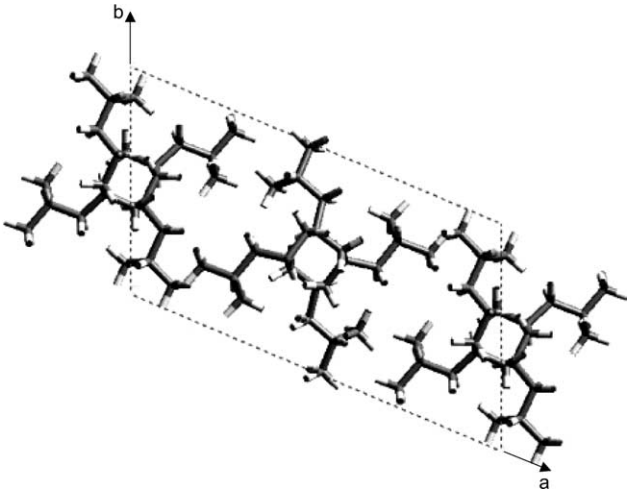

Fig. 9. The final structure of P4MP1 Form II made of antichiral isocline chains ($P112_1$ symmetry), as seen in *c*-axis projection. The different cell symmetry modifies the position of the origin of the unit-cell.

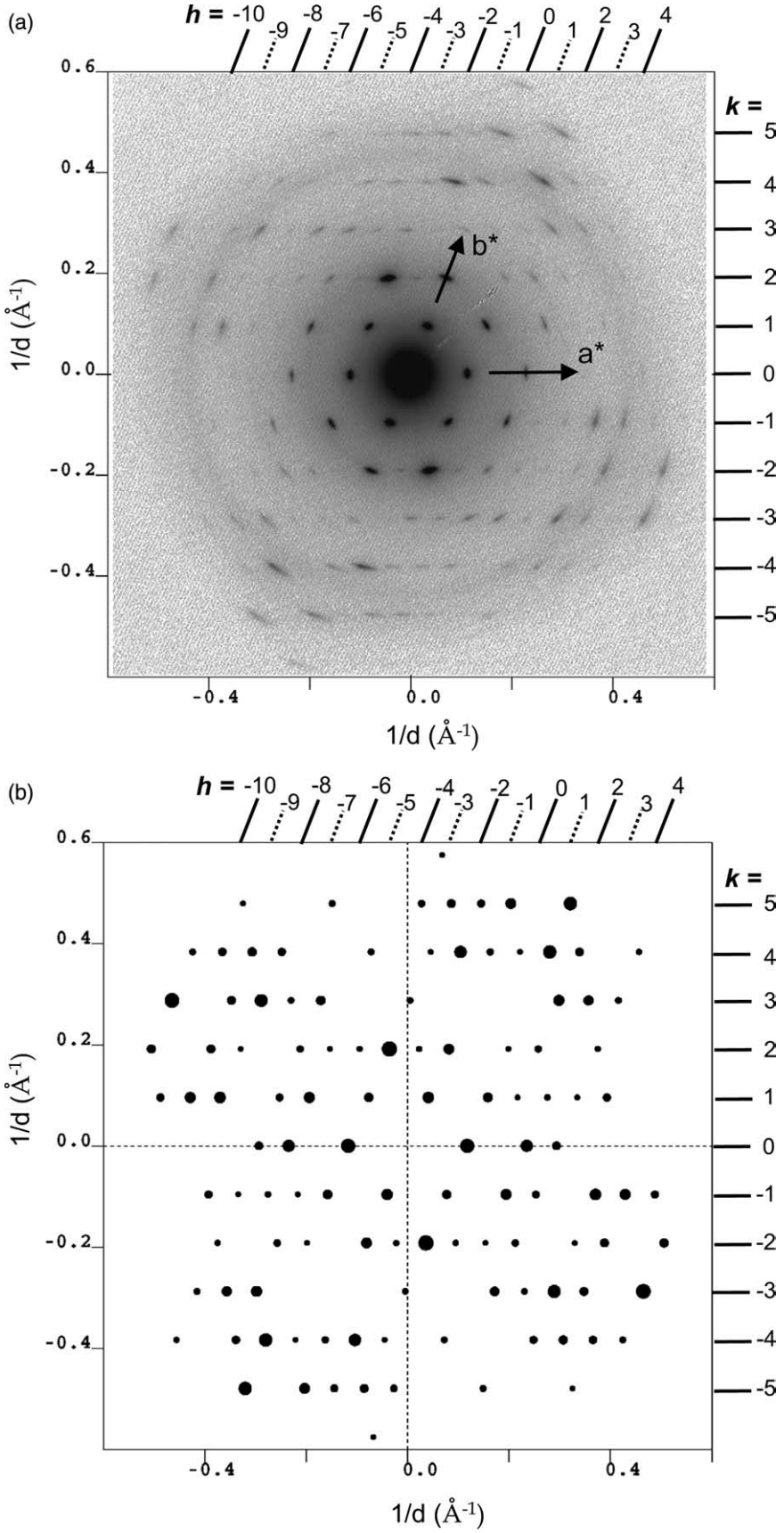

Fig. 10. (a) The diffraction pattern of Form II with intensities displayed in logarithmic scale (through image processing using the AnalySIS software). The critical weaker reflections are enhanced. (b) The calculated diffraction pattern of the model displayed in Fig. 9. Note in both cases the presence of *hk*0 reflections with *h* odd, indicating that the two chains have different *c*-axis projections and azimuthal settings.

c-axis projections, all *hk*0 reflections with *h* odd are absent (cf. Figs. 5, 6 and 8).

The more detailed diffraction patterns shown in Figs. 2(b) and 3(b) display, however, several reflections with *h* odd (cf. also later, Fig. 10(a)). The corresponding layer lines are indicated by dotted lines in Fig. 2(b) and 10(a). The most prominent ones are $\bar{1}40$, $\bar{7}10$, $\bar{7}30$ (with spacings ≈ 2.5 Å^{-1}) but there are a number of weaker reflections ($\bar{1}20$, 3*k*0, etc.). These reflections do not result from electron diffraction artifacts: double diffraction, or 'bleeding' of reflections from upper layer lines (e.g. *hk*1), as a result of limited lamellar thickness. They are consistently observed, essentially with the same intensity relative to their *hk*0 (*h* even) neighbors. They are definitely not streaks: their angular spread compares well with that of their *h* even neighbors. They point therefore to a genuine, or at least a representative feature of the crystal structure that has been overlooked so far. In essence, they indicate that, although the unit-cell does indeed contain two helices, the *c*-axis projections of these two helices are not identical. For the polyolefins considered here, this in turn indicates that the two helices that coexist in the unit-cell cannot be both enantiomorphous and anticline, as implied by the $P2_1/a$ space group (we recall that enantiomorphous implies miror-related shapes, i.e. conformations, which is more specific than antichiral, that only describes the opposite helical hands). The $P2_1/a$ symmetry is only a possible (perhaps an ideal), but in fact not the actual cell symmetry.

A plausible modification of the structures considered so far takes advantage of the fact that anticline isochiral helices are nearly isosteric: a given 'up' helix can be replaced by the same helix oriented 'down' with relatively little steric 'damage'. This modification is similar to, but different from the statistical unit-cell considered above, since only one stem site is involved, and the resulting stem packing is not a statistical one. In the present case, such a substitution generates a unit-cell that contains two isocline antichiral helices, in which the two helices have different *c*-axis projections, as suggested by the additional *hk*0 reflections. However, the substitution is not straightforward, in view of the low symmetry of the unit-cell. In essence, the reversed chain must adapt to a more 'hostile' environment, since the orientation of the *a*-axis is not that expected for this 'upside down' chain (thus the change of conformation, and the loss of 'enantiomorphism'). Since, also the two helices are no longer related by a center of inversion, the new symmetry of the unit cell becomes $P112_1$ (space group number 4).

This substitution has again been modeled by conformational and packing energy analysis. The results depend to some extent on the vagaries of the minimization procedure and on the characteristics of the initial model (azimuthal setting of the chains, etc.). Significantly, an energy-minimized structure (Fig. 9) reproduces many features (chain conformation and azimuthal settings) that were present in the two initial $P2_1/a$ symmetry crystal structures shown in Figs. 5(a) and 7(a). In essence, the cell contains a helix of one hand of the model considered in Fig. 5(a) and the antichiral helix of the model contained in Fig. 7(a). As indicated, the symmetry of the unit-cell is now $P112_1$, and the two fold helical symmetry still applies for each of the two stems. The diffraction pattern calculated for this amended crystal structure displays some interesting characteristics (Fig. 10(b)). In particular, it features (as expected) the additional *hk*0 (*h* odd) reflections observed in Fig. 2(b). Fig. 10(a) displays this same pattern, but with the intensity on a logarithmic scale in order to better reveal the weaker reflections (overall, 50 independent reflections are visible). The calculated $\bar{1}40$,$\bar{7}10$, $\bar{7}30$ reflections are the strongest of the *hk*0 (*h* odd) reflections, as observed experimentally. Many other features of the diffraction pattern, notably in its periphery (which is more sensitive to the small changes in atomic coordinates that differentiate the initial and the present model) are well reproduced: presence of the rows of 3*k*0 and 5*k*0 reflections (*k* even and odd), etc. Note that the experimental electron diffraction pattern includes reflections up to 0.6 Å^{-1} (or 1.7 Å in direct space): the agreement reached between the calculated and the experimental pattern is thus a very demanding test for any structure derivation.

The structure is again reached by an energy minimization procedure, and has no short steric contacts. The packing energy is -144.8 kcal/unit-cell (Table 2, third line), which compares well with the models with $P2_1/a$ symmetry considered earlier. In view of its highly improved consistency with the experimental diffraction pattern, this low symmetry structure with two isocline antichiral stems is a better model for P4MP1 Form II. To conclude this structure derivation, we report the atomic coordinates of Models 1 and 2 in Table 3 and those of the final model in Table 4. Also, besides the graphical comparison of *hk*0 intensities displayed in Fig. 10(a) and (b), the main features of the powder pattern are indicated in Table 1, where they are compared with the data of Charlet and Delmas [6].

Table 3
Coordinates for the tentative $P2_1/a$ models of P4MP1, Form II

Atoms[a]	Model 1[b]			Model 2[c]		
	x/a	*y/b*	*z/c*	*x/a*	*y/b*	*z/c*
$C_1(H_2)$	0.742	0.618	0.323	0.687	0.401	0.669
$C_1(H)$	0.719	0.592	0.531	0.672	0.424	0.464
$C_1(H_2)$	0.666	0.670	0.591	0.583	0.364	0.419
$C_1(H)$	0.711	0.829	0.623	0.543	0.204	0.408
$C_1(H_3)$	0.768	0.860	0.788	0.454	0.154	0.410
$C_1(H_3)$	0.653	0.897	0.657	0.569	0.146	0.237
$C_2(H_2)$	0.676	0.434	0.570	0.710	0.580	0.412
$C_2(H)$	0.680	0.396	0.778	0.732	0.606	0.205
$C_2(H_2)$	0.609	0.259	0.828	0.733	0.747	0.137
$C_2(H)$	0.531	0.280	0.860	0.653	0.758	0.121
$C_2(H_3)$	0.531	0.351	1.046	0.664	0.907	0.065
$C_2(H_3)$	0.461	0.139	0.853	0.597	0.653	0.984

[a] Main chain atoms in bold. Indices to the carbon atoms differentiate the two monomers of the crystallographic repeat unit. Full coordinates: x, y, z; $-x+1/2, -y, z+1/2$; $-x, -y, -z$; $x+1/2, y, -z+1/2$.

[b] Model as shown in Fig. 5(a).

[c] Model as shown in Fig. 7(a). For both models 1 and 2, monoclinic unit-cell, space group $P2_1/a$ (# 14, option 4). Parameters: $a=18.50$ Å, $b=10.43$ Å, $c=7.22$ Å, $\gamma=113°$. The statistical model (Fig. 8(a)) has same coordinates, but occupancy factor 1/2.

Table 4
Fractional coordinates of P4MP1 Form II

Atoms[a]	Chain 1			Chain 2		
	x/a	*y/b*	*z/c*	*x/a*	*y/b*	*z/c*
$C_1(H_2)$	0.012	0.389	0.648	0.569	0.584	0.653
$C_1(H)$	0.034	0.412	0.441	0.577	0.552	0.447
$C_1(H_2)$	0.088	0.340	0.379	0.663	0.579	0.396
$C_1(H)$	0.050	0.179	0.371	0.721	0.732	0.384
$C_1(H_3)$	−0.011	0.127	0.216	0.701	0.811	0.227
$C_1(H_3)$	0.113	0.118	0.345	0.805	0.738	0.356
$C_2(H_2)$	0.072	0.570	0.399	0.524	0.399	0.400
$C_2(H)$	0.069	0.609	0.194	0.501	0.376	0.194
$C_2(H_2)$	0.134	0.752	0.147	0.481	0.224	0.133
$C_2(H)$	0.218	0.757	0.134	0.549	0.175	0.119
$C_2(H_3)$	0.277	0.909	0.213	0.515	0.019	0.068
$C_2(H_3)$	0.229	0.675	−0.034	0.612	0.258	0.977

Final model, as shown in Fig. 9. Monoclinic unit-cell, space group $P2_1$ (full name: $P112_1$, number 4, option 2). Parameters: $a=18.50$ Å, $b=10.43$ Å, $c=7.22$ Å, $\gamma=113°$.

[a] Main chain atoms in bold. Indices to the carbon atoms differentiate the two monomers of the crystallographic repeat unit. Full coordinates: x, y, z; $-x, -y, z+1/2$.

4. Discussion

The above structure derivation started with the presentation of two models that differ from the final model. This indirect approach is explained by the fact that we had to rely initially on a less detailed electron diffraction pattern. These models were also introduced because they turn out to be of interest when considering the cell symmetry of polyolefin crystal structures. First, however, we compare Form II and Form III of P4MP1. We also note that the structure derived here fully supports the concept of 'symmetry breaking' discussed in detail in the paper by De Rosa [1] and in his review on this topic [18].

4.1. Crystal structures of Forms II and III of P4MP1. Transitions to Form I

The structure derivation of Form II of P4MP1 parallels strikingly that of Form III due to De Rosa et al. [7], even more so than the recent analyis of Form II [1], De Rosa et al. [7] also had to discard models of Form III in which inappropriate combinations of clinicity/chirality of the four chains in the unit-cell did not fit the experimental single crystal electron diffraction pattern recorded by Charlet et al. [5] and Pradère et al. [8]. As seen in Fig. 11, we are dealing in both cases with isocline antichiral stems in the cell. In Form III, there are four chains in the cell and isocline antichiral helices are found along the two crystallographicaly equivalent *a* and *b* directions. All interactions between stems are mainly of the 'face-to-face' type, which is typical of interactions between antichiral helices. In the present Form II, there are only two chains in the cell (two cells are represented in Fig. 11) and the 'face-to-face' interactions occur only along the *a*-axis (It is for this very reason that an alternate model made of isochiral anticline stems (e.g. Right up–Right down) that would have the same *c*-axis projection as our model can be discarded: it has very severe steric conflicts) (Fig. 12).

In both Form II and Form III, twinned structures are possible. Although Form III has a tetragonal cell, the twinned components differ by the clockwise or counter-clockwise rotation of the chains in the unit-cell relative to the *a* or *b* axes. Twinned single crystals of Form III were investigated by Pradère et al. [8]. The monolayer, twinned single crystals are frequently multiple twins in which the twinned microsectors are bounded by (100) and/or (110) twin planes. Existence of these twins was a major indication in the structure derivation and helped De Rosa et al. [7] select the correct $I4_1$ space group out of several possibilities. In Form II, twinned structures are expected in view of the monoclinic unit-cell and have been

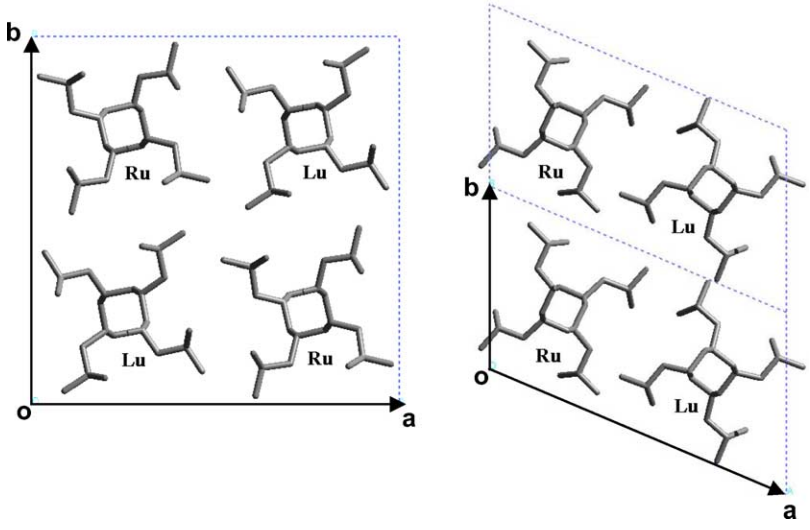

Fig. 11. Comparison of the crystal structure of Form III of P4MP1, as established by De Rosa et al. [7] and that of Form II (cf. Fig. 9; the origin of the cell has been shifted to ease comparison with the tetragonal unit-cell). Note the alternation of antichiral isocline helices along both *a* and *b* axes of the Form III cell, and a similar alternation only along *a* in Form II.

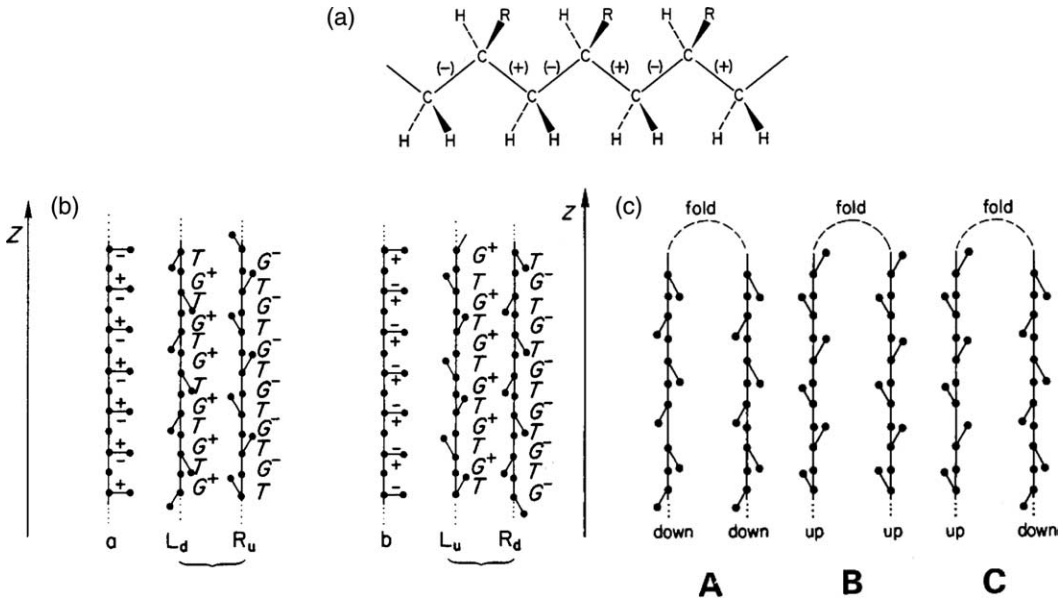

Fig. 12. The constraints set by chain folding on the clinicity/tacticity of stems linked by a fold, as analyzed by Sadler et al. [13] and by Petraccone et al. [14] (drawings reproduced from [14]). (a) The succession of (+) and (−) conformations in a chain. (b) The helices (clinicity/chirality) generated by the two favored conformations (TG^+ or G^-T) applied to the (+)(−) sequence of bonds. (c) All possible relative clinicities of isotactic polyolefin stems linked by a fold and that obey the criteria defined in parts (a) and (b). Stems linked by a fold differ either by their chirality or by their clinicity, but not by both. Thus, in models A and B, the two stems are antichiral whereas in model C, they are isochiral.

observed in the present investigation (cf. Fig. 3). Interestingly, in the two different twin components, the exact conformation of any one chain depends on its combined chirality/clinicity. It is easily understood that the reasoning developed in Fig. 6 still applies for the model with $P112_1$ symmetry. Considering the twinned components' unit-cells drawn in Fig. 3(b), cell 1 corresponds to the structure as drawn in Fig. 9. It is thus made of Left-Up helices as in Model 2 and Right-Up helices as in Model 1 (or, equivalently, Right-Down of Model 2 and Left-Down of Model 1). In the twinned component (cell 2 in Fig. 3), the above model numbers are reversed. In other words, equivalent helices (say Right up) have (if only slightly) different conformations in the different components of the twin. This analysis thus illustrates the symmetry-breaking concept detailed by de Rosa, in this case the stringent adjustment of the individual stem conformation (chirality/clinicity) to the local crystallographic environment (in the twinned crystal, the local orientation of the *b*-axis). By contrast, the twins in Form III differ only by the azimuthal orientation of the stems relative to the *a* or *b* axes, but not by the conformation of any individual stem.

Takayanagi and collaborators [4] have observed that both Forms III and II are converted to Form I by a solid-solid phase transition at high temperature. They investigated these phase transitions by various techniques: IR spectroscopy, dilatometry, viscoelastic behavior. The transitions take place at about 75–80 and 120–130 °C ((III–I and II–I, respectively). [4] Charlet et al. [5] investigated by electron microscopy and diffraction the III–I transformation using single crystals: they observe the development of cracks in the square crystals of Form III, associated with the slight lateral contraction of the unit-cell (from 19.4 to 18.7 Å) upon transition to the more extended chain conformation of Form I. It is known that a (solid-state) crystal–crystal transformation between two different crystal structures with helical chain conformation maintains the helical hand of the individual stems, as demonstrated for the Form II–I transformation of isotactic poly(1-butene) [19]. Since, the unit-cells of both Forms III and I are tetragonal with full antichiral packing of helices along the *a* and *b* axes, virtually no stem movement takes place during the III–I phase transition, apart from the helix geometry change. By contrast, the II–I transformation implies more significant molecular movements, in which the nearest neighbor isochiral stems along the *b*-axis of Form II become second nearest neighbors in a tetragonal packing, whereas the ⟨120⟩ direction becomes the new *b*-axis of the tetragonal unit-cell (cf. Fig. 11). These more important rearrangements may explain the higher temperature (by ≈40 °C) at which the II–I transformation takes place, compared to the III–I one.

In order to further compare Forms III and II, we included in Table 2 the results of a conformational and packing energy analysis of the various structures that have been considered. The overall (including intra- and inter-molecular terms) and van der Waals energies are compared under the same minimization protocol. The three different models considered for Form II (using the experimentally determined cell parameters, three first lines) have already been compared. The final model ($P112_1$ symmetry) has slightly lower total energy than Models 1 and 2 ($P2_1/a$ symmetry). Its total energy is comparable to that of Form III (here obtained with the unit-cell determined by De Rosa et al. but after minimization of their structure with our set of potentials). To parallel our analysis of Form II, we have also included in this Table an alternative model of Form III with $I4_1/a$ space group (made of

antichiral anticline helices) that was discarded by de Rosa et al. because it was inconsistent with the diffraction data, and has poorer interdigitation of the side-chains [7]. Our results support these conclusions.

Reverting to Form II, we note that the above comparison may not be appropriate for Models 1 and 2, since their unit-cell may differ from the experimentally determined one that, strictly speaking, applies only for the model with $P112_1$ symmetry. We have therefore, launched another round of minimizations in which the unit-cell parameters are not constrained to the experimental values. The corresponding results are reported in the lower half of Table 2, for the three models of Form II and for the two models of Form III. The results should be considered with reservation since the potentials used are, expectedly, not able to reproduce the very low packing density characteristic of P4MP1: the density of all minimized models increases by nearly 10% compared to the experimental one. Also, the computed energies are very similar. In particular, the computed energy of the experimentally observed Form III is again comparable to that of Form II in its various modifications ($P2_1/a$ and $P112_1$ symmetries). Attempting nevertheless an analysis of these results, we note that the monoclinic cell geometry is preserved in the Form II, and does not revert to Form III. Further, the chain axis repeat does increase for the observed Form II crystal structure, compared with that of Form III, in agreement with the early observations of Takayanagi and collaborators [4]. The scatter in *c*-axis repeats in the minimized structures is surprising, although short helix periodicities are known for four fold helices of polyolefins (polyvinylcyclohexane has a 6.5 Å *c*-axis periodicity). It indicates that the very finer details of the structure cannot be established reliably by conformational energy analysis only. The set of potentials does not seem to be the major problem: it has been used to analyze other, established crystal structures of polyolefins, and reproduces them adequately. Judging from these variations (and some inadequacies between observed and calculated intensities), some details of the present structure derivation may need further refinement, although the major novelty of the model (its low symmetry) is well established.

Among models with $P2_1/a$ symmetry, Model 2 seems to be preferred over Model 1, and compares favorably with the structure with $P112_1$ symmetry. It is therefore probable that in the actual structure, the stems that 'represent' Model 2 determine the geometry of the cell (i.e. the orientation of the *a*-axis). Following the analysis developed in Fig. 6, they are the 'hosts' in the unit-cell, and stems of Model 1 are the 'guests' that must adapt to the less favorable orientation of the *a*-axis imposed by these 'host' stems. This situation (in which one chain dictates its rule and another one must adapt to an environment that is not its preferred one) defines very clearly a situation of packing 'frustration' that involves in the present case two antichiral helices. It is thus different from the frustration that involves three chains and leads to trigonal cells with three chains per cell, exemplified in polymer crystal structures of isotactic polypropylene ((β) phase), of syndiotactic polystyrene ($(\alpha)''$ structure), etc. In both cases, however, we are dealing with a combination of symmetry breaking and frustration.

4.2. Crystal structure symmetry of polyolefins: chirality and clinicity issues

An original feature of the present structural investigation of P4MP1 Form II is the low cell symmetry ($P112_1$) and the fact that the helices are isocline: the two chains in the monoclinic cell are not related by a 'logical' crystallographic element of symmetry, such as an inversion center. It is thus of interest to consider the issues of chirality and clinicity in the broader context of helical polyolefins crystal structures.

Isotactic polyolefins do not have a chemical sense, which should make the issue of stem orientation irrelevant (as in e.g. polyethylene). However, the conformational features of these 'chiral but racemic' polymers brings both chirality and clinicity into play. Therefore, up- and down-, combined with right- and left-handed helices may coexist in any crystal structure. Analysis of the synergies and/or the mutual exclusions of the various combinations have been an ongoing theme of the crystallography of polyolefins.

The chirality of the helices is a stringent requisite in the buildup of the unit-cell. Many polyolefin crystal structures associate enantiomorphous (antichiral) helices: the cell has a mirror or a glide plane as in isotactic polypropylene, α phase. In tetragonal unit-cells, the packing is usually fully antichiral along both *a* and *b* axes. However, some polyolefin structures are chiral, as e.g. poly(1-butene) in its form III (orthorhombic cell, $P2_12_12_1$ symmetry) [17,20], or when they exist in chiral, frustrated crystal structures [21–24].

Clinicity is usually considered as a less stringent requisite than chirality. Ordering in the up–down organization of helices is a feature of crystallization at higher temperatures, when slower growth allows for better selection of the depositing chain or reorganization of the deposited stems. The resulting lower symmetry of the cell is sometimes difficult to demonstrate experimentally (for the α phase of isotactic polypropylene, it is manifested by additional reflections on the first layer line of the (fiber) pattern, but not on the equator). At lower crystallization temperatures, up- or down-pointing isochiral helices can occupy a given stem site because they are nearly isomorphous. Statistical unit-cells are thus frequently observed, especially for fast crystallization or growth rates. The statistical up–down substitution precludes of course any investigation on a possible relationship between the clinicity of neighbor helical polyolefin stems.

Such a relationship does, however exist, as first analyzed by Sadler et al. [13] and later by Petraccone et al. [14] in the mid-1980s. These authors point out that the chirality and clinicity (relative up- or down-orientation) are not independent for helical stems linked by a fold (in the following, we will consider tight folds that link nearest neighbor stems, and assume that they are a representative or significant fraction of the folds and loops). In essence, the rule is the following: stems linked by a fold differ either by their chirality or their clinicity; folds can link Right up and Right down, or Right up and

Left up. The chirality and the clinicity cannot differ together: Right up and Left down helices cannot be linked by a fold.

Using the formalism developed by Corradini [25] and summarizing the reasoning of Petraccone et al. [14], the conformations of the two bonds attached to the substituted carbon atom can be distinguished by (+) and (−). (+) bonds tend to adopt G^+ or T conformations, (−) bonds G^- or T conformations (or stay in the corresponding troughs of the conformational energy map). Only successions of G and T are sterically favored, which leaves G^+T or TG^-. The allowed combinations not only define the helical hand (G^+T and TG^- induce left- and right-handed helices, respectively), but also the tilt of the C_α–C_β bond relative to the helix axis—i.e. define a directionality [14]. As stated by Sadler et al. [13], 'the molecule has acquired a quasi-chirality'. Because of the link (fold), the chirality of one stem imposes directionality to the next stem, or the directionality of one stem imposes chirality to the next stem. Through its connection with chirality (that is defined by the crystallography), clinicity becomes a requisite as stringent as chirality in the build-up of the crystal. In a sense, the clinicity requisite is as stringent as those applying to chemically 'polar' polymers (e.g. polyamide 6, polyesters, or polypeptides).

In many helical polymers, packing of antichiral helices is energetically more favorable, which leaves one alternative only: the stems must be isocline. For chiral crystal modifications of polyolefins to the contrary, anticlinicity must be the rule. This justifies e.g. the $P2_12_12_1$ symmetry of form III of isotactic poly(1-butene) (orthorhombic cell, two anticline helices per cell) [17,20]. We note that it must also be operative in the chiral, frustrated phases that contain three chains per cell (e.g. β modification of isotactic polypropylene [21–23], etc.). Since, the odd number of stems is not compatible with regular ('crystallographic') up–down ordering, the clinicity issue could be an unavoidable source of structural disorder, that is indeed a frequent characteristic of frustrated structures.

Based on the above analysis, Sadler et al. [13] and Petraccone et al. [14,26] proposed folding patterns in isotactic polystyrene and isotactic polypropylene, respectively. In both models, the folds 'knit' together neighbor planes ((300) for iPS, (040) for iPP) that are known, from the crystal symmetry, to be made of antichiral helices. The helices within each layer of the bilayer linked by folds are isocline, which may be at variance with recent analyses of the structure of iPP [27]. Also, the folds are not parallel to the growth plane; half of them are even normal to it in iPP, which appeared difficult to reconcile with the fold orientation suggested by polyethylene decoration [28].

The constraints imposed by folds may not, by themselves, account for the cell symmetry. Form III of P4MP1 has, like Form II, isocline antichiral stems [7]. This stem organization may well result from packing considerations alone since it ensures a better interdigitation of side-chains [7]. The packing energy analysis of the two alternative structures, with $I4_1$ (antichiral isocline) and $I4_1/a$ (antichiral anticline) symmetries, both with fixed and variable cell parameters, support this view (cf. above and Table 2). Also, the unit-cell is tetragonal, i.e. does not differentiate fold- and non-fold planes, which is consistent with the prevalance of packing features over fold constraints. If the latter were the determining factor, the crystal symmetry would be reduced to orthorhombic. Note that this distinction is different from (although it may contribute to) the usual and well-documented 'mechanical' impact of folds on cell dimensions (as opposed to symmetry) in single crystal growth sectors. Bassett for example indicates that the inter-stem distance in fold planes of P4MP1 Form I is about 1‰ larger than in non-fold planes [11].

Form II of P4MP1 provides yet another opportunity to investigate the impact of chain folds on crystal symmetry. Its rare (for isotactic polyolefins) monoclinic unit-cell geometry alleviates the ambiguity between fold- and non-fold planes just mentioned for the tetragonal unit-cell of Form III. It also allows determination of the combined clinicity/chirality relationship between stems. Recalling briefly our observations:

–The monoclinic cell is made of antichiral but isocline helices.
–Alternative cells with antichiral anticline helices ($P2_1/a$ symmetry) are not observed although one variant at least has comparable conformational and packing energies (with all due reservation linked with the approximations involved).
–The low symmetry of the crystal structure is consistent with the existence of chain folds and the associated constraints on combined chirality/clinicity of stems linked by folds.
–The single crystals have well developed lateral *ac* faces, which is consistent with the orientation of folds suggested by the unit-cell structure. (Note, however, that these *ac* planes are also the densest crystallographic planes, and therefore likely growth faces, irrespective of the fold organization).

The symmetry of the Form II cell does not take advantage of the 'chiral but racemic' character of the chain. Precedence of the $P112_1$ symmetry of the unit-cell (i.e. antichiral isocline helices) suggests that the constraints set by folds on the chirality/clinicity of isotactic polyolefin stems, contribute to, or perhaps even determine, the cell symmetry. Usually, in the structure analysis of helical polyolefins, these constraints are difficult to demonstrate experimentally due to e.g. the impact of structural up–down disorder, which appears to be more frequent in cells the symmetry of which differs from that of the helices they house (e.g. Form I of P4MP1, tetragonal cell, 7_2 helices). When the cell and helix symmetries match (Form II of P4MP1, Form III of isotactic poly(1-butene)) their impact is more easily accessible to experimental check.

5. Conclusion

The structure of Form II of P4MP1, a polymorph first observed in 1966 [4], has been derived (for the second time, two years after the work of De Rosa! [1]) mostly from single crystal electron diffraction patterns combined with available X-ray powder patterns. Molecular modeling (conformational and packing energy) and comparison with single crystal electron diffraction patterns have been used to select

appropriate structures. Some major features of the Form II crystal structure have been either confirmed (cf. [1]) or uncovered.

–The chains are two fold helices that include four monomer units. The cell is monoclinic, which is highly unusual for P4MP1 and more generally for polyolefins with long side chains.
–Different structures have been considered. These are two variants with a $P2_1/a$ symmetry of the cell, that house two (crystallographically equivalent) enantiomeric and anticline helices, and their statistical combination. They account for some of the main features of the electron diffraction pattern, and for the powder X-ray diffraction pattern that was only available to De Rosa [1]. However, finer features revealed only by a more detailed electron diffraction pattern require that a different structural model must be considered, in which the two stems are indeed antichiral (but no longer enantiomorphous), and isocline. The cell symmetry is reduced to $P112_1$ and the correspondence of the calculated $hk0$ pattern with the experimental single crystal pattern is much improved.
–This departure from the 'logical' $P2_1/a$ crystallographic symmetry is consistent with the fact that the two adjacent stems in the cell are linked by a fold. As proposed by Sadler et al. [13] and by Petraccone et al. [14] the folds constrain the stems that are linked to be either anticline and isochiral, or antichiral and isocline. The latter situation, which results in a better packing, is observed in the present crystals.
–The morphology of the lamellar crystals is consistent with the structural model. The single crystals formed in thin films have well developed *ac* faces. These are precisely the faces in which the fold constraints impose antichiral isocline stems.

Constraints imposed by folds in isotactic polyolefins are quite general, although they have been discussed only on two occasions in the mid-1980s [13,14] and have been mostly overlooked in more recent works. This loss of interest probably stems from the fact that their manifestations are frequently blurred and their identification rendered difficult by structural disorder (up–down substitution of helices at any one site).

As a final comment, we note that this contribution suggests the possible existence of different variants of the same P4MP1 Form II crystal structure that depend on morphological features. The higher $P2_1/a$ symmetry variants with antichiral and enantiomorphous chains (Fig. 5 or, based on our energy analysis results, more probably Fig. 7) may be formed when the impact of folds is absent or reduced, as in e.g. extended-chain oligomers and, possibly, fibers. The antichiral, isocline variant retained in this study (Fig. 9, $P112_1$ symmetry) is more suitable (is mandatory?) when the polymer is part of a chain folded, lamellar crystal. The latter structure is of low symmetry and displays symmetry-breaking features since the two helices have different conformations. The structure also displays an original form of frustration since one helix defines its most appropriate environment (i.e. orientation of the *b*-axis of the cell) and the other helix adapts to that environment. However, the structure is not a disordered one, since the relative stem conformation and organization are highly defined.

References

[1] De Rosa C. Macromolecules 2003;36:6087.
[2] Frank FC, Keller A, O'Connor A. Philos Mag 1959;8:200.
[3] Kusanagi H, Takase M, Chatani Y, Tadokoro H. J Polym Sci Polym Phys Ed 1978;16:131.
[4] Kawasaki N, Tanda Y, Takayanagi M. Rep Progr Polym Phys Jpn 1966;9: 167. Kawasaki N, Takayanagi M. Rep Progr Polym Phys Jpn 1967;10: 337. Tagayanagi M, Kawasaki N. J Macromol Sci Phys 1967;B1:741.
[5] Charlet G, Delmas G, Revol JF, St John Manley R. Polymer 1984; 25:1613.
[6] Charlet G, Delmas G. Polym Bull 1982;6:367. Charlet G, Delmas G. Polymer 1984;25:1619.
[7] De Rosa C, Borriello A, Venditto V, Corradini P. Macromolecules 1994; 27:3864. De Rosa C, Auriemma F, Borriello A, Corradini P. Polymer 1995;36:4723. De Rosa C, Capitani D, Cosco S. Macromolecules 1997; 30:8322.
[8] Pradère P, Revol JF, St John Manley R. Macromolecules 1988;21:2747.
[9] Rastogi S, Hoehne GWH, Keller A. Macromolecules 1999;32:8897. Rastogi S, Newman M, Keller A. J Polym Sci, Part B Polym Phys 1993; 31:125.
[10] De Rosa C. Macromolecules 1999;32:935.
[11] Bassett DC. Phil Mag 1964;10:595.
[12] Khoury F, Barnes JD. J Res Nat Bur Std (US) 1972;76A:225.
[13] Sadler DM, Spells SJ, Keller A, Guenet JM. Polym Commun 1984;25:290.
[14] Petraccone V, Pirozzi B, Meille SV. Polymer 1986;27:1665.
[15] Cerius 2 User Manual; Accelrys, San Diego (CA, USA), Cambridge (UK).
[16] Ferro DR, Brückner S, Meille SV, Ragazzi M. Macromolecules 1990; 23:1676.
[17] Cojazzi G, Malta V, Celotti G, Zanetti R. Makromol Chem 1976;177:915.
[18] De Rosa C. Materials chirality. In: Green MM, Nolte RJ, Meijer EW, editors. Topics in Stereochemistry 24. New York: Wiley; 2003.
[19] Kopp S, Wittmann JC, Lotz B. J Mater Sci 1994;29:6166.
[20] Dorset DL, McCourt MP, Kopp S, Wittmann JC, Lotz B. Acta Crystallog. 1994;B50:201.
[21] Meille SV, Ferro DR, Brückner S, Lovinger AJ, Padden FJ. Macromolecules 1994;27:2615.
[22] Stocker W, Schumacher M, Graff S, Thierry A, Wittmann JC, Lotz B. Macromolecules 1998;31:807.
[23] Dorset DL, McCourt MP, Kopp S, Schumacher M, Okihara T, Lotz B. Polymer 1998;39:6331.
[24] Cartier L, Spassky N, Lotz B. Macromolecules 1998;31:3040.
[25] Corradini. In: Ketley AD, editor. The stereochemistry of macromolecules, vol. 3. New York: Marcel Dekker; 1968. p. 1960.
[26] Petraccone V, Pirozzi B, Meille SV. Eur Polym J 1989;25:43.
[27] Auriemma F, Ruiz de Ballesteros O, De Rosa C, Corradini P. Macromolecules 2000;33:8764.
[28] Wittmann JC, Lotz B. J Polym Sci, Polym Phys Ed 1985;23:205.